Representing atmospheric moisture content in the mountains: Examination using distributed sensors in the Sierra Nevada, California

Shara I. Feld

A thesis

submitted in partial fulfillment of the

requirements for the degree of

Master of Science

University of Washington

2012

Committee:

Jessica D. Lundquist

Alan F. Hamlet

Program Authorized to Offer Degree:

Civil and Environmental Engineering

University of Washington

Abstract

Representing atmospheric moisture content in the mountains: Examination using distributed sensors in the Sierra Nevada, California

Shara I. Feld

Chair of the Supervisory Committee:

Dr. Jessica D. Lundquist

Civil and Environmental Engineering

Atmospheric moisture content is a critical factor in both the water balance and the energy balance for a river basin. Despite its importance to hydrology, atmospheric moisture is sparsely measured, particularly in the mountains. Since few observations exist, numerous empirical methods have been developed to estimate relative humidity (RH) or the dewpoint temperature. However, most of these algorithms were developed in continental regions and may have limited accuracy outside the region where they were developed. Furthermore, future changes in atmospheric moisture content may reduce our ability to rely on empirically determined relationships. Alternative options include installing more in situ sensors, looking at nearby free air measurements, and/or running a numerical weather model.

We compared densely-distributed measurements of dewpoint temperatures in two study sites over three years in a semi-arid, maritime mountain range (Sierra Nevada, California) against: (1) simple empirical algorithms, (2) the Parameter-elevation Regressions on Independent Slopes Model (PRISM) linear regression data sets based on observational data, (3) the Weather Research and Forecasting (WRF) mesoscale model, and (4) radiosonde data. Empirical algorithms that used only one sea-level measurement of dewpoint to extrapolate to higher elevations, on average overestimated moisture in the basin, displaying median biases of daily dewpoint temperatures up to 10.5°C. These algorithms were subject to errors both from misrepresenting the linear rate of moisture loss with elevation and, on some days, from assuming the dewpoint temperature followed a linear pattern at all. These methods used assumptions that were empirically-derived in other climates. PRISM improved upon these methods by using local observations to determine the local average lapse rate, with median bias values of -0.3°C and 2.2°C in our study sites.

Empirical algorithms that derived dewpoint from air temperature showed a significant seasonal variation in performance. Assuming uniform advection of moisture from the Pacific does not capture the moisture dynamics in the Sierra Nevada. Radiosonde readings showed large biases from observations, and a wide range of day to day error. WRF improved on the free-air data, performing well in representing both the overall trends in the basin (with median biases of -0.9°C and -1.0°C in our study sites) and displaying the smallest range of error throughout the year. The impact of errors in dewpoint temperature estimation on hydrology is by applying the Distributed Hydrology Soils and Vegetation Model (DHSVM) to the upper Tuolumne River Watershed in Yosemite. A ±2°C bias in dewpoint temperatures resulted in an average ±3 day shift in snowmelt timing and change annual streamflow volumes by ±1%.

When modeling a geographically simple basin, one base station within the basin paired with PRISM lapse rates will be representative of overall moisture trends most of the time, biased by -0.3°C in one study site. However, if the basin is more geographically complex, with air masses varying due to predominant weather patterns, micro-topography, and transport along the mountain range, a physically-resolved model such as WRF is necessary to represent dewpoint variations. To reduce average modeled bias in a basin, the simplest method is to add a high-elevation station that records dewpoint temperatures and use that to model the average dew point temperature decline with elevation.

ACKNOWLEDGEMENTS

I would like primarily to thank my thesis advisor Dr. Jessica Lundquist for her guidance. I am fortunate to have received the opportunity to work with such an excellent mentor. In addition I would like to thank my committee member Dr. Alan Hamlet. Contributions to this work came from Nicoleta Cristea in calibrating and running the DHSVM model, Mark Raleigh and Courtney Moore for help with instrument deployment and retrieval, Nic Wayand and Mimi Hughes for help with WRF data acquisition and processing and the UW mountain hydrology research group for answering research questions and paper revisions. Funding was provided by NSF through grant number CBET-0838166, and by NOAA through their Hydrometeorological Testbed and through the Joint Institute for the Study of the Atmosphere and Ocean (JISAO) under NOAA Cooperative Agreement Nos. NA17RJ1232 and NA10OAR4320148. I would finally like to thank my family for their encouragement.

TABLE OF CONTENTS

Page

LIST OF FIGURES

LIST OF TABLES

1. Introduction

Atmospheric moisture content, typically measured as dew point temperature or relative humidity (RH), is a critical factor in modeling both the energy balance and the water balances in a river basin. Atmospheric moisture affects the energy balance by influencing both incoming longwave radiation and latent heat transfer [*Ruckstuhl et al.*, 2007]. Algorithms used to estimate longwave radiation, which is infrequently measured, rely on air temperature and water vapor in the atmosphere [*Flerchinger et al.*, 2009]. Because increased water vapor raises the emissivity of the earth's atmosphere, higher dewpoint values in the atmosphere result in more incoming longwave radiation at the surface [*Rangwala et al.*, 2009]. Dewpoint measurements are particularly important in making accurate empirical estimates of longwave radiation when clouds are present [*Sicart et al.*, 2006]. At the same time, a smaller dewpoint depression, the difference between the air temperature and the dew point temperature, results in reduced evaporation or sublimation and thus less surface cooling due to latent heat. Inaccurate longwave radiation and energy balance estimates can change the modeled timing of snowmelt and the estimated energy available for potential ET, affecting the projected water balance for agricultural and urban uses.

Dewpoint depression also affects the water balance by changing the amount of water evaporated or transpired from a basin. Evapotranspiration (ET) increases with a greater dewpoint depression, as there is a greater deficit between the moisture that the atmosphere can hold and the current moisture content. The Penman-Monteith equation, which can be used to predict ET, is strongly affected by changes in dewpoint depression, as well as being influenced by the estimated longwave radiation [*Gong et al.*, 2006].

Despite its importance to hydrology, atmospheric moisture is sparsely measured. Data limitations are exacerbated at higher elevations in complex terrain. In California, the number of meteorological stations per hundred-meter elevation band declines significantly with elevation above sea level [*Lundquist et al.*, 2003]. Of the available mountain meteorology measurements, only a small fraction record atmospheric moisture variables. For example, in the SNOTEL network, a system of high elevation weather stations maintained by the National Resources Conservation Service for water supply and snowmelt, only about 14% of over 800 stations around the western U.S. measure relative humidity [http://www.wcc.nrcs.usda.gov/snow/ Accessed 2 November 2011].

Given limited available measurements, numerous empirical algorithms have been developed for projecting RH or dew point temperatures across mountainous terrain. These range in complexity from simple extrapolations to more extensive calculations that require iterative schemes. These empirical algorithms are available for two cases: 1) no measurements are available in a watershed [*Kimball et al.*, 1997; *Running et al.*, 1987], and 2) only one point measurement is available, which must be distributed across a basin [*Cramer*, 1961; *Franklin*, 1983; *Kunkel*, 1989; *Wigmosta and Vail*, 1994]. Most of the algorithms available were developed in continental regions, such as western Montana [*Running et al.*, 1987], New Mexico and Texas [*Kunkel*, 1989]. *Kimball et al.* [1997] notes that algorithms developed in arid locations have limited accuracy in regions outside where they were developed. For example, *Waichler and Wigmosta* [2003a] found that when generating meteorological data in the Oregon Cascades, using the minimum temperature for daily dew point did not generate the observed RH pattern as well as using historical observations of monthly and hourly RH means to make future projections. *Eccel* [2012] found that while the widely used methods [*Kimball et al.*, 1997;

Running et al., 1987] were appropriate in the Italian alps, site-specific calibrations based on month and presence of precipitation were required.

Furthermore, our future ability to rely on relations determined empirically from historical observations is limited with changes in atmospheric moisture. Dew point temperatures have increased by several tenths of a degree per decade across most regions of the U.S. during 1961 - 1995, reflecting an increase in atmospheric water vapor [*Gaffen and Ross*, 1999; *Robinson*, 2000; *Trenberth,* et *al*. 2007]. While relative humidity trends are weaker, these reflect increases across the country as well [*Gaffen and Ross*, 1999]. Climate model projections indicate that the water vapor content of the atmosphere will continue to increase in the future [*Dai et al.*, 2001; *Trenberth,* et *al*. 2007].

Given the importance of atmospheric moisture content in hydrological modeling and the sparsity of measurements in mountain locations, this paper investigates options for representing RH or dew point temperatures in the Sierra Nevada. These mountains are an apt study location for two reasons. First, prior work hints that RH may be more difficult to estimate in semi-arid or Mediterranean climates, the climate classification of our test basins according to *Peel et al.* [2007]. Second, the Sierra Nevada, where our test sites are located, is of particular concern to water resource managers, as there are significant future water supply shortages projected [*Barnett, et. al.*, 2008].

To understand different measures of atmospheric moisture content and how they change in complex terrain, we first review these variables (2). We next present the study area and data sources used (3.1). We present a summary of methods to estimate dew point temperatures in a mountain basin when limited or no observations are available (3.2). These include: (a) simple empirical algorithms, (b) the Parameter-elevation Regressions on Independent Slopes Model

(PRISM), which uses lapse rates based off observations [*Daly et al.*, 2008], (c) the Weather Research and Forecasting (WRF) model, which is a numerical weather prediction system [*Michalakes et al.*, 2001], and (d) using data from a nearby radiosonde station. These methods were selected to test the transferability of empirical fits to our study site (empirical methods), whether physical principles of conservation of moisture in a lifted air mass are an appropriate metric for the basin, whether uniform advection of the free atmosphere describes moisture dynamics in the mountain range (radiosonde data), or whether a full atmospheric physics model is necessary to capture dewpoint variations (WRF). Methodology includes a summary of analysis techniques (3.3). The results (4) first summarize with a case study (4.1), then look at the performance of these models in representing atmospheric moisture in the study sites (4.2), and look into factors affecting their performance (4.3). We demonstrate the impacts of errors in representing this meteorological input of atmospheric moisture on timing of snowmelt and quantity of streamflow (4.4). This work can provide guidelines for choosing methods to represent atmospheric moisture content in the Sierra Nevada and similar regions.

2. Background: Metrics of Atmospheric Water

Water vapor is influenced by the air temperature and the local atmospheric pressure, which change with elevation according to the ideal gas law. Atmospheric moisture content may be expressed in numerous ways. The mixing ratio (R) defines the mass of water in the atmosphere per kilogram of dry air. The actual vapor pressure of water (E_a) defines the amount of water in the air in units of pressure, while the saturation vapor pressure (E_{sat}) is the amount of water that the air can hold at a given temperature. The relative humidity (RH) is the ratio of the actual over the saturation vapor pressure. The dew point temperature (TD) is the temperature at which the air will be saturated for a given amount of water vapor. The difference between this and the actual air temperature is termed the dewpoint depression. Further explanation on these variables and how they can be calculated is given in Appendix A.

Figure 1 illustrates relations between measures of atmospheric moisture when holding dewpoint temperature, mixing ratio or relative humidity constant with changes in elevation. In panel (A), we use cups of water to visualize atmospheric moisture (adapted from *Cramer* [1961]). The size of the cup is the potential amount of water that the air can hold at a given temperature. The amount of moisture in the air is represented by the water in the cup. As elevation increases, pressure and temperature decrease, in turn decreasing the overall size of the cup. Panel (B) shows dewpoint temperature (TD), mixing ratio (R), actual vapor pressure (Ea) and relative humidity (RH) with changes in elevation. When dewpoint temperature is held constant with elevation, water vapor pressure remains constant, while RH increases due to decreasing air temperature, and the mixing ratio increases due to pressure changes with elevation. When the mixing ratio is held constant with elevation, vapor pressure and dewpoint temperatures decline slightly, while RH increases with elevation. When RH is held constant

with elevation, the dew point temperature, actual water vapor, and dew point depression decrease with elevation.

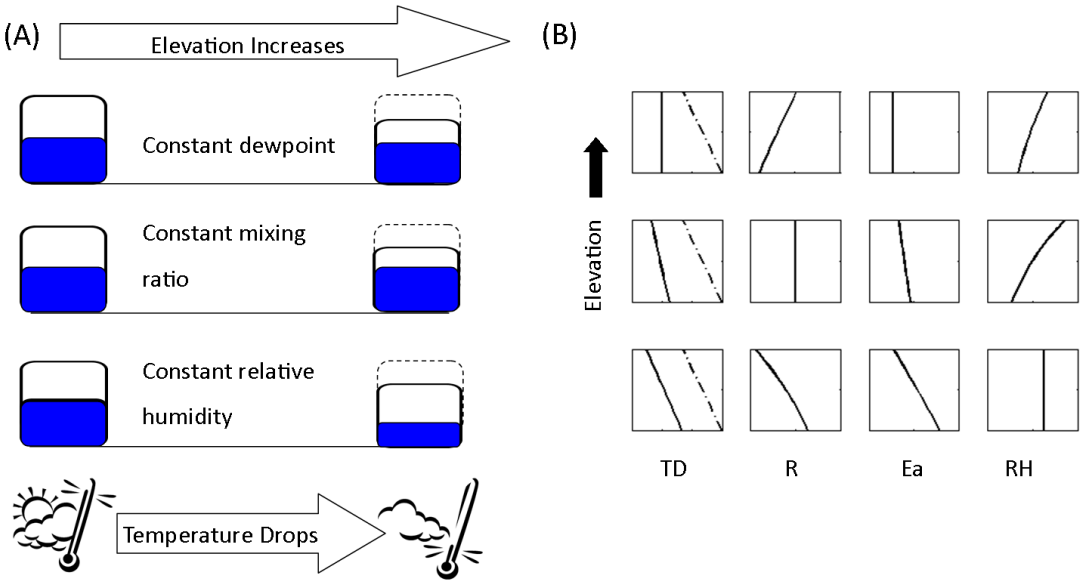

Figure 1. Schematic representation of relationship between atmospheric water vapor metrics with changes in elevation. (A) Visual representation of maintaining constant dewpoint temperature, constant mixing ratio, and constant relative humidity with increases in elevation and the corresponding decrease in temperature. Cups representing saturation vapor pressure contain water representing actual vapor pressure. (B) Dewpoint temperature (*TD*) with dashed line for air temperature, mixing ratio (*R*), actual vapor pressure (*Ea*) and relative humidity (*RH*) with changes in elevation for constant dewpoint temperature (top row), constant mixing ratio (*R*) and constant relative humidity (middle row).

For this study, we represent atmospheric moisture with dew point temperature for three reasons. First, dew point temperature is familiar to water resource managers as the most commonly used humidity measure [*Gaffen and Ross*, 1999; *Robinson*, 1998], and is the metric used in numerous models [*Daly et al.*, 1994; *Kimball et al.*, 1997; *Running et al.*, 1987]. Quality control techniques used for air temperature can be applied easily to dew point temperature. Second, dew point temperature most frequently shows a clear lapse rate at elevation. Third, dewpoint is a conservative property with isobaric heating and cooling as long as there are no moisture changes [http://amsglossary.allenpress.com. Accessed 8/16/12].

3. Methods

3.1. Study Area and Data Sources

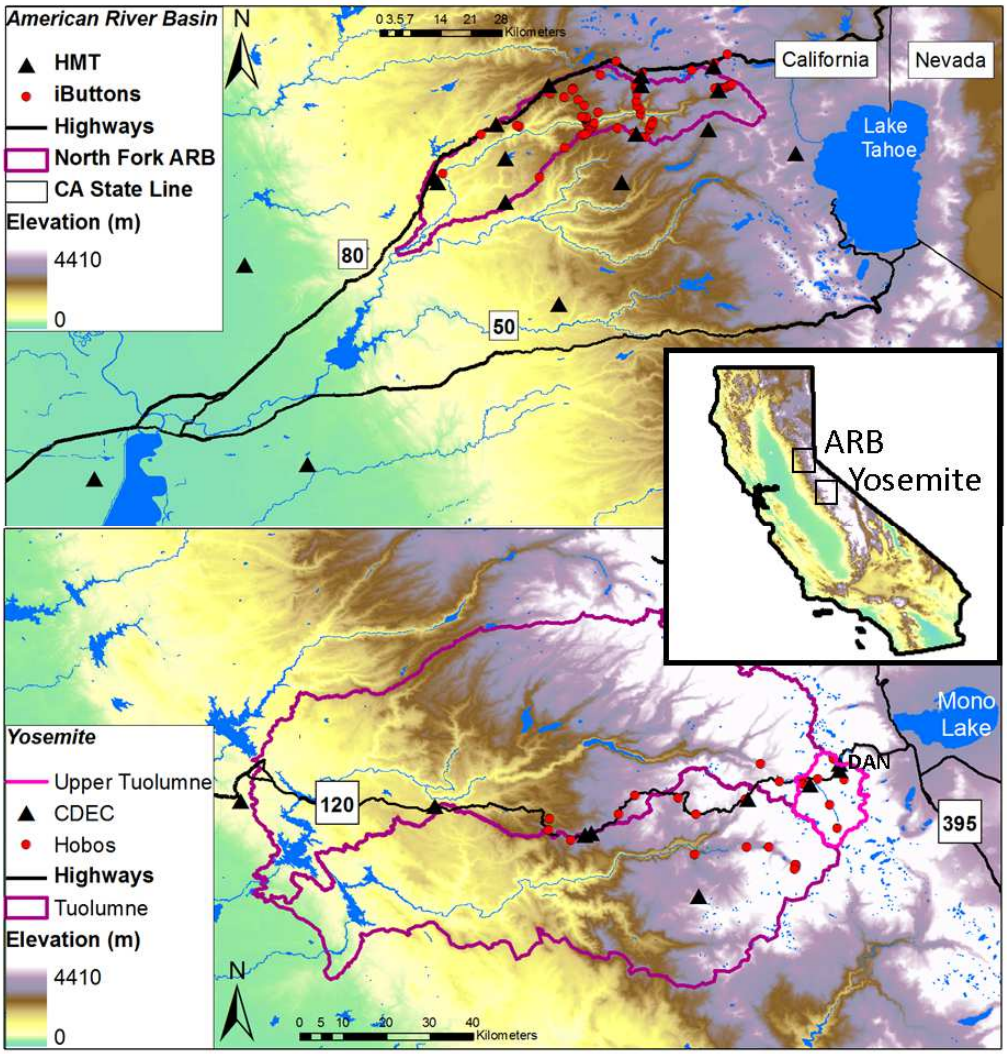

Figure 2. Maps of (a) the American River Basin (ARB) and (b) the Tuolumne and Merced River Basins in the vicinity of Yosemite National Park. Watersheds that are highlighted include the North Fork American River Basin in the ARB, the Tuolumne in the Yosemite area, and the Upper Tuolumne River Basin above Highway 120. The locations of permanent meteorological towers (HMT stations in the ARB and CDEC stations in Yosemite) and temporary sensors (iButtons in the ARB and Hobos in Yosemite) are shown. The Dana Meadows station (DAN), used for hydrologic modeling impacts (described in section 3.3) is shown.

Table 1. Observational Data

Region	Measurement	Period of record (water years)	Count of stations	Elevation Range (m)
ARB	Hydrometeorological Testbed Stations	2008 – 2010	15	7-2100
ARB	Hygrochron iButtons	2008-2010	64	424-2429
Yosemite	CDEC stations	2003-2005	9	311-3031
Yosemite	Hobo sensors	2003-2005	25	1309-3205

We assessed the performance of methods of generating dewpoint temperature in the Sierra Nevada in California. Two well-instrumented study sites were selected on the west slope of the Sierra Nevada to represent two variations on topographic controls. These are the North Fork American River Basin (ARB), where elevation increases fairly uniformly from west to east, and the Yosemite area, which contains multiple sub-basins that experience cold air pooling effects and deviations from linear air temperature lapse rates [*Lundquist and Cayan*, 2007; *Lundquist et al.*, 2008] (Fig. 2). The Sierra Nevada receives the majority of its precipitation in the winter and early spring and little during the summer. Annual precipitation and runoff fluctuate between 50% and 200% of the climatological averages [*Lundquist and Cayan*, 2007]. In the Sierra Nevada, water vapor contributions are from the Pacific Ocean for most of the year [*Dodd*, 1965; *Robinson*, 1998]. On a coarse scale dewpoint temperatures decreased between Sacramento and a high elevation meteorological station in the Sierra Nevada [*Dodd* 1965]. Air masses over the east slope are much drier, moving off the Nevada desert.

We used data from permanent meteorological towers and hygrochron iButtons [http://www.maxim-ic.com/datasheet/index.mvp/id/4379] in the ARB. Permanent

meteorological towers from elevations between 7 and 2100 meters in the ARB were part of the NOAA Hydrometeorology Testbed (HMT). The HMT is a meteorological measurement program aimed at providing data for improved hydrologic forecasting [*Ralph et al*, 2005], with measurements sampled every two minutes for water years 2008 through 2010. A high-resolution network was created with hygrochron sensors, a stand-alone device that measures air temperature and RH and records the data in an enclosed data logger. Precipitation measurements were also acquired from the HMT stations. Hygrochrons were installed in evergreen trees 1.5 to 4 meters above the ground (depending on local snow depth) and shaded from the sun by overhanging branches. Further radiation shielding was provided by upside-down plastic funnels. Deployment methodology followed *Lundquist and Huggett* [2008]. The hygrochrons were deployed each August and recorded data every two hours for approximately 11 months until reaching capacity, for subsets of water years 2008 through 2010. An average of 35 hygrochrons were deployed each water year over the study period, representing 64 locations that ranged in elevation from 424 to 2429. Appendix B details a validation study on deploying hygrochrons in remote conditions.

We used data from permanent meteorological towers and Hobo sensors [http://www.onsetcomp.com/products/hobo-data-loggers] in Yosemite. These data run an east-west transect across the ridge line of the Sierra Nevada. Data from permanent meteorological towers at elevations from 311 to 3031 meters were acquired from the California Department of Water Resources Data Exchange Center (CDEC), a hydrometeorological data program in California originally started for flood forecasting [http://cdec.water.ca.gov/intro.html]. The CDEC stations provided hourly air temperature, relative humidity and precipitation data for water years 2003 through 2005. Hobo sensors were deployed between May and June at

elevations from 1309 to 3205 meters for one to two years at a time for water years 2003 through 2005, recording data every 15 to 30 minutes [*Lundquist et al.*, 2003]. An average of 20 hobos were deployed each water year over the study period, representing 25 locations that ranged in elevation from 424 to 2429 up the west slope of the Yosemite study site. All data were quality controlled using the methodology of *Meek and Hatfield* [1994]. This included removing extreme spikes in the data, values outside of the threshold of operation, and long periods of constant data records that were not consistent with nearby stations in the basin. For analysis, data were averaged into daily-average and monthly-average timeseries, when at least 75% of the time period was available.

3.2. Methods of Estimating Dew Point Temperatures

3.2.1. Empirical Algorithms: Projecting Dewpoint From a Base Station

Table 2. Empirical algorithms: spatial projections of dewpoint measured at a base station. One dewpoint measurement available.

Model	Test Location	Model Description	**Citation Count**
Cramer [1961]	Western Oregon	Assumes constant mixing ratio with elevation.	3
Franklin [1983]	Priest River Experimental Forest in northern Idaho	Dew point lapse rate of -1.25 °C km^{-1} with elevation.	32
Kunkel [1989]	Validated at 11 stations in the intermountain West.	Dew point calculated from base station dew point ($e(z_o)$)) adjusted by the difference between site elevation (z) and base elevation (z_o) and a constant based on the month (a_m) $e(z) = e(z_0)\exp[-a_m(z - z_0)]$	18
Constant RH Wigmosta et al. [1994]	DHSVM model is employed widely. RH distribution is included in the hydrologic model.	Relative humidity is constant throughout the basin.	860

Citation count acquired from Google Scholar, 4/9/12.

Where a single point measurement of moisture content exists, empirical algorithms use data from a base station and make assumptions about the variation of moisture across an elevation gradient to project dewpoint temperatures to sites in the basin. The following algorithms can be used to spatially extrapolate moisture content (Table 1). *Cramer* [1961], a study in western Oregon, assumes thorough mixing between air layers, which results in a constant mixing ratio (and thus atmospheric water content) with elevation. The mixing ratio is conserved during adiabatic lifting of an air parcel [*Wallace and Hobbs*, 2006], so we would

expect this relationship if topographically-forced air is the primary cause of vertical moisture variation and no moisture condensation is occurring. *Franklin* [1983] used observations from the Priest River Experimental Forest in northern Idaho, and found that dew point temperature varied with elevation according to a lapse rate of -1.25°C km^{-1}. *Kunkel* [1989], extrapolates water vapor pressure based on differences between site elevation and base station elevation. This is corrected with monthly-varying coefficients empirically calculated from 11 stations in the intermountain west; data is from the climate atlas of the US [*NOAA*, 1968]. This algorithm thus fits a seasonally-varying empirical adjustment to declining water vapor pressure with elevation. Some models, such as the Distributed Hydrology Soils and Vegetation Model (DHSVM), assume a constant relative humidity, throughout a basin [*Wigmosta et al.*, 1994]; given that temperature decreases with elevation, this results in moisture declines with elevation. *Franklin* [1983] is cited as the lapse rate of choice in *Running et al.* [1987]. SnowModel, a snow evolution model, employs the *Kunkel* [1989] method for relative humidity extrapolations [*Liston and Elder*, 2006].

When utilizing empirical algorithms that project dew point temperatures from a base station, we must evaluate two metrics: (a) how well does the modeled lapse rate fit the observed lapse rate, and (b) how much does the location of the base station within the basin influence modeled results. The choice of base station from which to project dewpoint temperatures may be limited; often the only reliable source available is a low-elevation airport weather station. To investigate the performance of projecting dewpoint temperatures given standard available data, dewpoint temperatures were extrapolated from the Sacramento international airport weather station [http://cdo.ncdc.noaa.gov/ulcd/ULCD] to observation locations within the ARB and Yosemite.

3.2.2 Fitting Lapse Rates with Local Data: PRISM

The Parameter-elevation Regression Independent Slopes Model (PRISM) can be considered an optimal empirically-derived local lapse rate. The model incorporates observations into linear regressions to produce gridded datasets of climate parameters using the procedures described in *Daly et al.* [2008] for air temperatures to generate dewpoint temperature maps. Local lapse rates are defined and used to construct grids with observations from available stations that are weighted according to their similarity to their local grid cell. Continuous, digital maps at a resolution of 4-km are available for monthly average, minimum and maximum temperature, precipitation and dew point data on monthly, annual and event-based timescales. 800-m normals are also available for air temperature and precipitation [http://prism.oregonstate.edu/]. This data is similar to the empirical methods based on one atmospheric moisture measurement in a basin, except that this regression based on local observations. We acquired dew point for 4-km grid cells in the Yosemite area and the American River Basin for water years 2001 through 2010 and compared these to observations located within the grid cells.

3.2.3. Empirical Algorithms: Estimating Dewpoint From Air Temperature Alone

Table 3. Empirical algorithms: based off air temperature. No atmospheric moisture measurements in a basin.

Model	Test Location	Model Description	**Citation Count**
Running et al. [1987]	Montana (1983), Oregon (June 1989 – March 1990), WA, AK, TN, WI, AZ, FL (1984)	Dew point assumed to be minimum daily temperature.	383
Kimball et al. [1997]	Validated at 52 weather stations in the continental US from 1987-1994	Calculates dew point (*Td*) from min (*Tmin*) and max (*Tmax*) daily temperature and the ratio of daily evapotranspiration to annual precipitation (*EF*) (in Mt-Clim, 90 day annualized precipitation is used). $Td = Tmin[-0.12 + 1.211(1.003 - 1.444EF + 12.312EF^2 - 32.766EF^3) + 0.0006(Tmax - Tmin)]$	155

Citation count acquired from Google Scholar, 4/9/12.

When no atmospheric moisture measurements exist, empirical algorithms may use air temperature to estimate water vapor measurements (methods described in Table 2). *Running et al.*, [1987], developed primarily in Montana but since employed widely across the U.S., use the daily minimum temperature as the dew point temperature. This assumes that dew forms every night and at this point, given the high latent heat demands of condensation, further drops in air temperature below the dewpoint temperature will be reduced. *Kimball et al.*, [1997] note that the minimum nighttime temperature may be higher than the dewpoint temperature in arid climates, where dew may not form every night. Their algorithm, validated at stations across the US, expands upon the *Running et al.* [1987] method by adjusting the calculated dew point depending

on the aridity of the region, as measured by the ratio of the daily potential evapotranspiration to annual precipitation. To investigate performance of estimating dewpoint temperature from air temperatures, we used air temperature measurements from every observation in our study sites, and compared the local measured dewpoint with that estimated from local temperature.

The Variable Infiltration Capacity (VIC) model [*Liang et al.*, 1994], which has been widely used to solve water and atmospheric energy balances, and the Mt-Clim meteorological pre-processing model [*Glassy and Running*, 1994; *Kimball et al.*, 1997], both employ methods from the *Running et al.* [1987] and *Kimball et al.* [1997] algorithms. It should the noted that the Mt-Clim model uses a 90-day annualized precipitation for the aridity index in the *Kimball et al.* [1997] method. The Mt-Clim methods are employed in the RHESSys hydroecological model [*Tague and Band*, 2004] and the Advanced Weather Generator meteorological preprocessor [*Ivanov et al.*, 2007] for the TIN-based Real-Time Integrated Basin Simulator (tRIBS) [*Ivanov*, 2004]. The VIC preprocessor methods were applied to generate the widely-used *Maurer, E.P. et. al.* [2002] (cited 380 times, accessed 4/9/12) and *Hamlet, A.F. and D.P. Lettenmaier* [2005] (cited 160 times, accessed 4/9/12) atmospheric forcing datasets for hydrologic modeling.

3.2.4. Free-air Variations: Radiosonde Data

Free air dewpoint data were acquired from radiosonde measurements at Oakland, obtained from the NOAA radiosonde database [http://www.esrl.noaa.gov/raobs/]. Sounding data were available twice daily, at 00 and 12 UTC (16 and 4 local time). These data were averaged daily and interpolated to the elevation of observations in the ARB and Yosemite for comparison.

3.2.5. Physically-based Free-air Variations: WRF

The Weather Research and Forecasting Model (WRF) is a physically-based numerical weather prediction models that can be forced with observational data [*Skamarock and Klemp*, 2008]. Initial and lateral boundary conditions in the WRF product were forced with the 32-km gridded North American Regional Reanalysis (NARR), a meteorological product that incorporates surface and upper air observations, to a large extent radiosonde data, over the continental US [*Mesinger et al.*, 2006]. Boundary conditions were reinitialized every 5 days with an allowed three hours of spin-up. The WRF model is run at a six-second timestep, resolving vertical temperature and moisture profiles with advection from neighboring grid cells and using the Morrison 2-moment microphysics scheme [*Morrison et al.*, 2009]. To test the ability of WRF to represent spatial gradients of atmospheric moisture, the WRF model was run at 6-km resolution over California for October – June of water years 2001 – 2010. These data were prepared by Mimi Hughes of NOAA and are described in [*Hughes et al.*, submitted; *Wayand et al.*, submitted]. Running WRF at a 6-km grid size resolves local topography, such as the Sierra Nevada, at a scale useful for hydrological modeling. An advantage of WRF is that it is internally consistent: physical relations between air temperatures and dewpoint temperatures are maintained. Surface output of air temperature and relative humidity were acquired for 6-km grid cells across the Yosemite area and American River Basin for water years 2001 through 2010. We calculated dew point temperature from these data and compared these data to observations located within the grid cells to assess the performance of the model.

3.3. Hydrologic Model

The propagation of dewpoint estimation errors in hydrological modeling are demonstrated using the DHSVM hydrology model in a small basin in the Yosemite area. DHSVM is a physically-based distributed hydrology model that requires inputs of air temperature, relative humidity, wind speed, incoming shortwave and longwave radiation and precipitation at a three-hourly time step [*Wigmosta et al.*, 1994]. The input relative humidity is assumed constant over the basin. The model was calibrated for the sub-basins of the upper Tuolumne River Basin in Yosemite National Park for water years 2003 through 2009 [*Cristea et al.*, submitted; *Lowry et al.*, 2011]; we look at the small sub-basin of the Tuolumne River above Highway 120 (Fig. 2) with elevations ranging between 2600 and 4000 m . Baseline dewpoint temperatures were calculated using temperature and relative humidity measured at the Dana Snow Pillow Site at 3000 m elevation (Fig. 2). These were adjusted to represent uniform biases of ±2°C. In cases where adjusting the dewpoint temperature up by 2°C caused the dewpoint to exceed the air temperature, the dewpoint temperature was capped at the air temperature (to prevent unphysical conditions of super-saturation). This was necessary in 15% of the total time-steps, resulting in an average dew point temperature increase of 1.85°C. Longwave radiation was calculated using the *Idso* [1981] algorithm for clear sky conditions. Evapotranspiration, latent heat fluxes, streamflow and SWE generated by the model were compared to values generated using locally-measured (baseline) dewpoint data. Sublimation rates were approximated from latent heat fluxes, using the latent heat of sublimation.

3.4. Techniques for Assessing Observed Dewpoint Patterns

We look at observed dewpoint temperature trends and concurrent meteorology to evaluate reasons behind the performance of the models. To assess the frequency of days with and without a linear pattern, we calculated a best fit line between daily dewpoint temperatures and elevation. The root mean squared error (RMSE) between observations and this best-fit line defines the amount of scatter from a linear lapse rate, where a low RMSE is a relatively linear dewpoint lapse rate with elevation while a high RMSE shows scatter in dewpoint temperatures with elevation.

The impact of precipitation on dewpoint temperature trends was determined by applying a binary to total daily precipitation. We assessed when measured precipitation in a day was greater than zero, as opposed to recording no precipitation at the permanent station.

To assess the influence of wind patterns we looked at the NOAA NCEP/NCAR reanalysis data sets [http://www.esrl.noaa.gov/psd/data/composites/day/ Accessed 27 July 2012]. These can be used to build composite data sets to see large-scale meteorological patterns. Vector wind composites were created at the 850 mb and 700 mb geopotential levels to illuminate wind patterns affecting the ARB and Yosemite area respectively. These composites were created for days with RMSE values <1°C, 1°C to 2°C and >3°C.

4. Results

4.1. Case study of Estimated Dewpoint Temperatures in the Sierra Nevada

We illustrate the performance of methods of generating dewpoint data with a case study in the ARB (Fig. 3) and Yosemite (Fig. 4). Here we show modeled dewpoint temperatures plotted against elevation. In both basins two days are shown, one day (left column) with a strong linear trend between dewpoint temperature and elevation, where better performance of the algorithms is expected, and one day (right column) with a weak trend between dewpoint temperatures and elevation.

Methods that estimate dewpoint temperatures from one point measurement in the basin (Fig. 3A, Fig. 4A) perform well when there is both a linear trend of observed dewpoint temperatures in the basin, and the algorithm lapse rate matches that trend. Both the assumption of a constant mixing ratio with elevation [*Cramer*, 1961] and of the almost equivalent -1.25°C km^{-1} lapse rate [*Franklin*, 1983] do not lose moisture quickly enough with gains in elevation. Adjustments to vapor pressure [*Kunkel*, 1989] or assuming constant RH with increases in elevation [*Wigmosta and Vail*, 1994] are closer to representing the decreased moisture at elevation, yet performance is limited by either the complex topography of Yosemite or days that do not show a linear lapse rate in dewpoint with elevation. The inclusion of PRISM [*Daly et al.*, 2008] shows the variation between observations and monthly-determined lapse rates within the ARB and Yosemite. While these lapse rates do not capture daily variability, the PRISM method of weighted observations does come close to reproducing large-scale moisture trends within the basin. Both assuming that the dewpoint is the minimum daily air temperature [*Running et al.*, 1987] and employing an aridity correction to this minimum temperature [*Kimball et al.*, 1997] may misrepresent daily moisture (Fig. 3B, Fig. 4B). Furthermore, if the basin contains few

stations, modeled data will be subject to compounded errors when dewpoint temperatures are projected across the basin. Radiosonde data do not always capture the moisture variations in the basin, indicating that humidity in the mountains cannot be well-predicted by the vertical structure of humidity atmospherically upstream (Fig. 3C, Fig. 4C). The WRF mesoscale model [*Skamarock and Klemp*, 2008] is shown to perform well in both cases in the ARB and Yosemite.

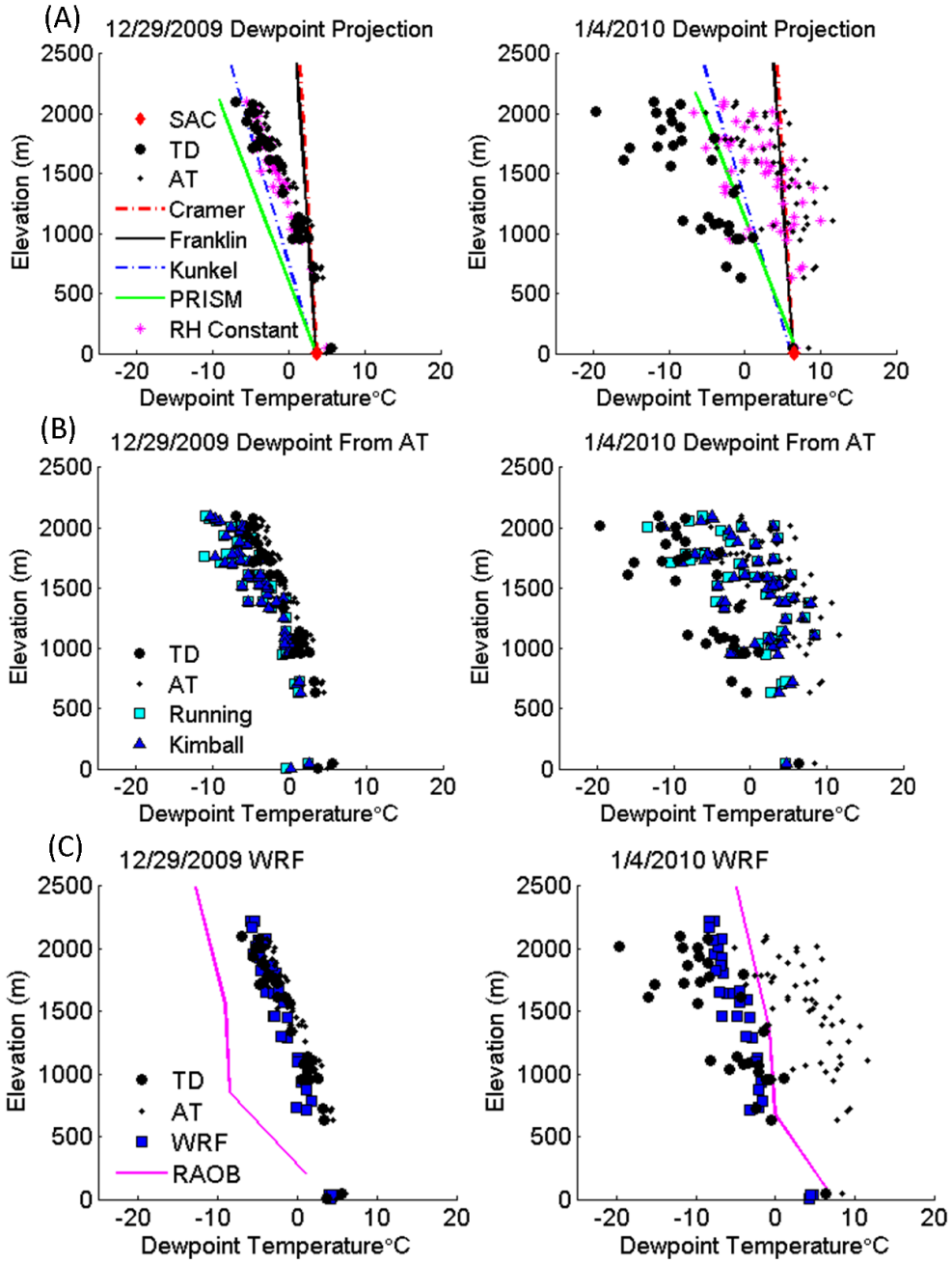

Figure 3. Case study in the American River Basin of estimated dewpoint temperatures on a day showing a linear trend in dewpoint temperatures with elevation (left column) and a day showing a weak trend of dewpoint temperatures with elevation. Observed dewpoint temperatures (TD) and air temperature (AT) are shown. (A) Estimation of dewpoint temperature from the Sacramento (SAC) airport station (constant mixing ratio with elevation [*Cramer*, 1961], -1.25°C km^{-1} lapse rate [*Franklin*, 1983], adjustments to vapor pressure [*Kunkel*, 1989], constant RH with increases in elevation [*Wigmosta and Vail*, 1994]), and PRISM [*Daly et al.*, 2008] (B) estimation of dewpoint temperature from air temperature ([*Kimball et al.*, 1997; *Running et al.*, 1987]) and (C) the WRF mesoscale model [*Skamarock and Klemp*, 2008], and radiosonde data.

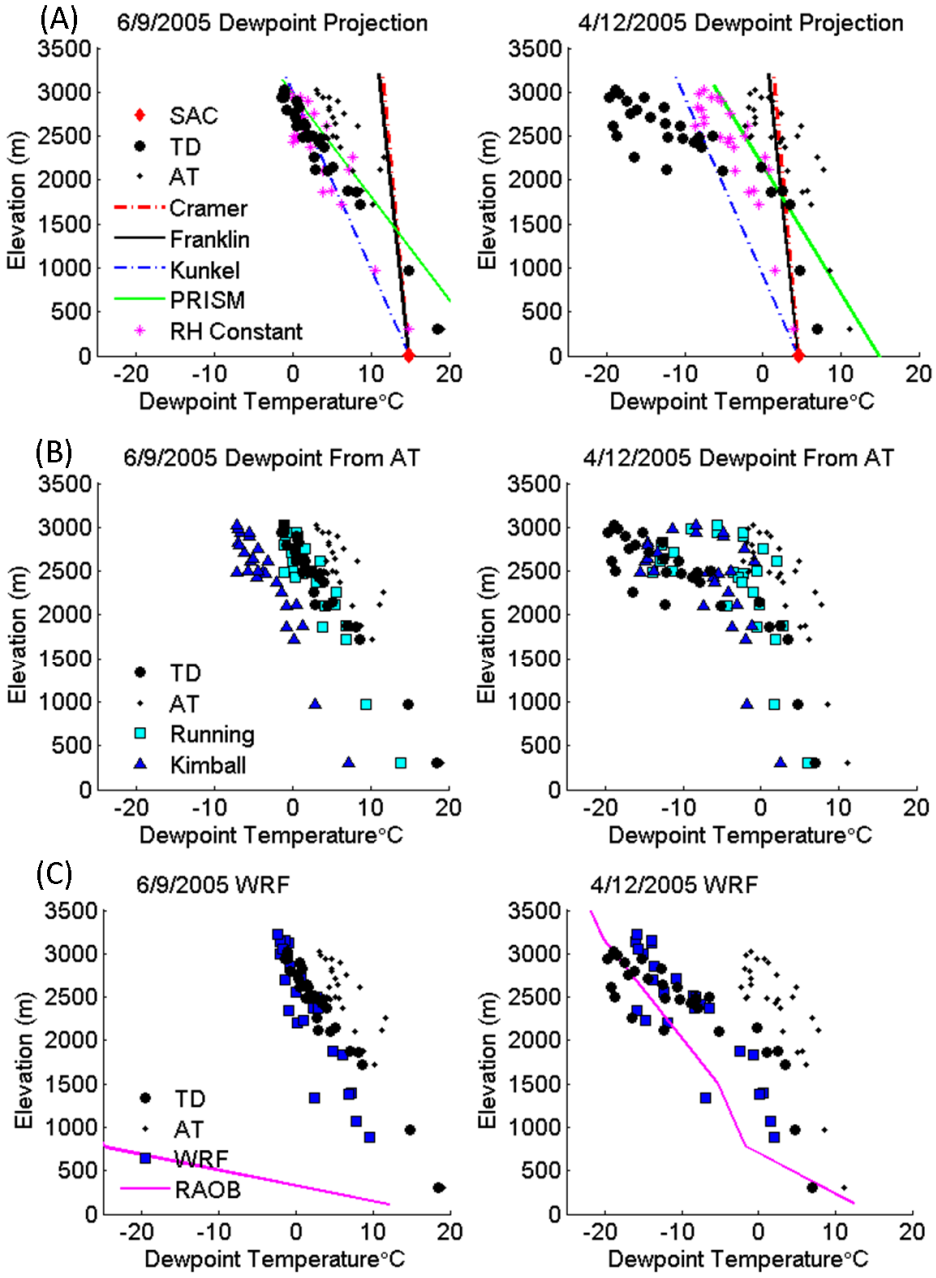

Figure 4. As in Fig. 3, except for Yosemite area.

4.2. Performance of Methods of Generating Dewpoint Temperatures in the Sierra Nevada

Figure 5 illustrates the performance of methods of generating dewpoint temperatures (a) within the ARB for water years 2008-2010 and (b) within the Yosemite area for water years 2003-2005, using histograms of the bias between daily-averaged modeled data and daily-averaged observations. Biases are calculated from the period for October through June to match the WRF period of record.

When one measurement of dewpoint temperature is available within a basin, empirical methods of extrapolation across a basin are dependent on both the choice of the base station, and whether the modeled lapse rate fits the observed lapse rate. Due to the typically limited availability of stations measuring dewpoint temperatures in mountain regions, we used the Sacramento airport station to represent available data. This station is near sea-level, an elevation below all stations within the basin. Assuming a constant mixing ratio with elevation [*Cramer*, 1961] results in a wet bias, with a median bias value of 4.7°C in the ARB and 10.5°C in the Yosemite area. The assumption of a –l.25°C km^{-1} dewpoint temperature lapse rate from the base station [*Franklin*, 1983] results in median wet bias values of 4.4°C in the ARB and 10.1°C in the Yosemite area. Seasonally-varying adjustments to the actual vapor pressure losses with elevation [*Kunkel*, 1989] are close to the trend of moisture loss in the basin, with a median bias value of -1.8°C in the ARB and 0.1°C in the Yosemite area. Assumptions of constant RH [*Wigmosta and Vail*, 1994] also represent moisture loss in the basin, however are dry-biased by -0.6°C in the ARB and wet-biased by 1.2°C in the Yosemite area. Much of the reported bias decreases when extrapolating from a measurement within the basin (not shown), suggesting that regardless of choice of method, errors are minimized by choosing a site as close to center of the desired elevation range as possible.

Since PRISM data [*Daly et al.*, 2008] is produced in monthly-average maps, we compare these data to monthly-averaged dewpoint temperatures. On this course resolution, the PRISM data performs better than other empirical techniques in the ARB. Figure 4 shows a median bias of -0.3 in the ARB and 3.4°C in the Yosemite area.

When no measurements of dewpoint temperature are available, the bias in dewpoint temperatures estimated from the air temperatures depends on the overall aridity of the basin. Assuming that the dewpoint temperature is equal to the nighttime minimum temperature [*Running et al.*, 1987] results in a median wet bias in both basins, of 1.8°C in the ARB and 0.9°C in the Yosemite area. Using an aridity correction on this minimum daily temperature [*Kimball et al.*, 1997] results in a median wet bias of 1.1°C in the ARB, while resulting in a median dry bias of -4.1°C in the Yosemite area.

Radiosonde data can be used to assess whether upwind upper-air measurements represent atmospheric moisture patterns within a basin. These data are dry-biased, with a median bias of -5.0°C in the ARB and -7.1°C in the Yosemite area.

The WRF model [*Skamarock and Klemp*, 2008] resolves atmospheric physics and dynamics, and matches observed dewpoint temperatures in both basins well, with a median bias of -0.9°C in the ARB and -1.0°C in Yosemite, for the time period of October through June.

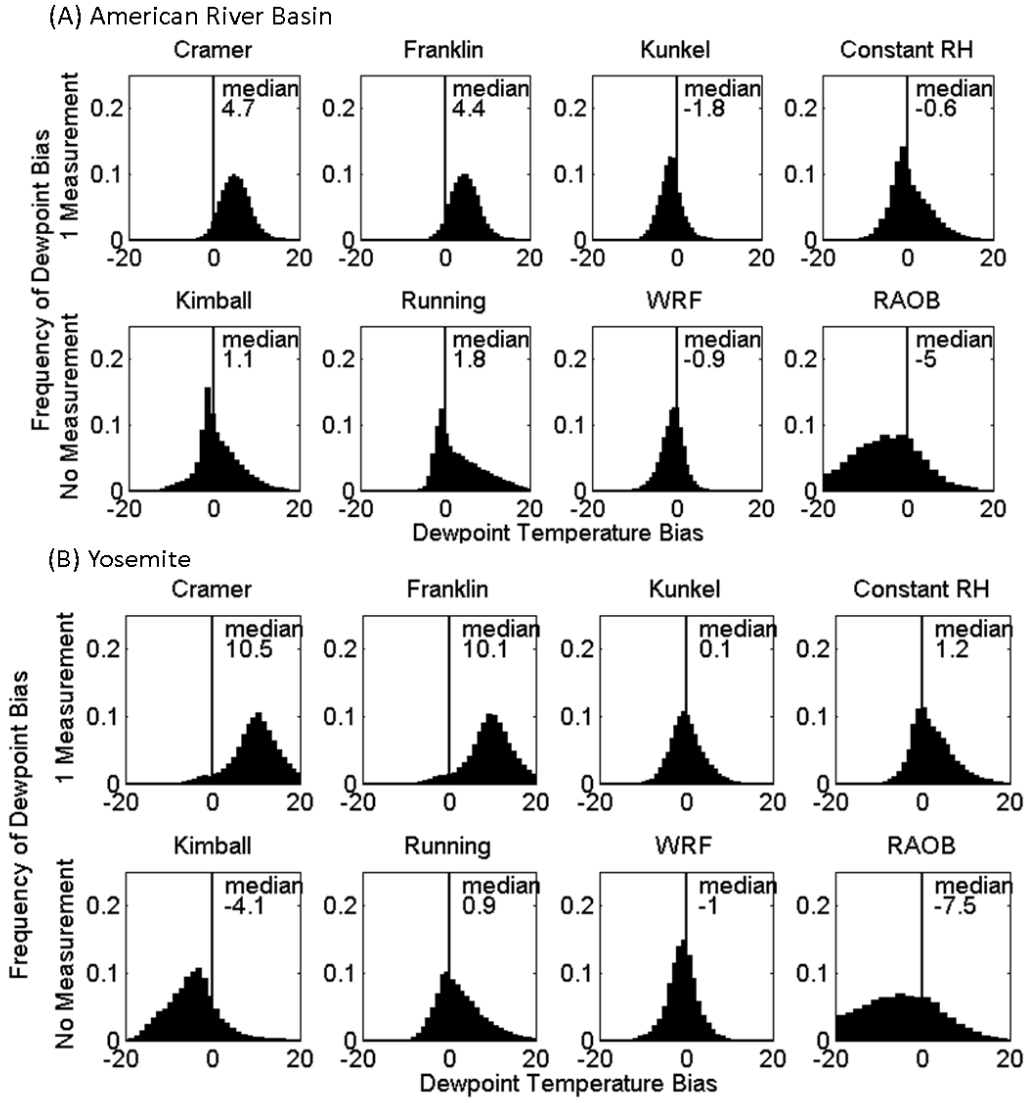

Figure 5. Performance of methods of generating dewpoint temperatures with daily-averaged data in (a) the ARB and (b) the Yosemite area. Methods of spatially-extrapolating dewpoint from one measurement in the basin include constant mixing ratio with elevation [*Cramer*, 1961], -1.25°C km^{-1} lapse rate [*Franklin*, 1983], adjustments to vapor pressure [*Kunkel*, 1989], constant RH with increases in elevation [*Wigmosta and Vail*, 1994], methods of estimating dewpoint temperatures with no available measurements include calculations from air temperature ([*Kimball et al.*, 1997; *Running et al.*, 1987]), the WRF mesoscale model (WRF) [*Skamarock and Klemp*, 2008], and radiosonde data. Note: WRF output was only available for October through June, although all other methods were evaluated for the entire period of record.

The interquartile ranges highlight likely errors in performance beyond the median bias. Figure 6 shows a boxplot of the bias between monthly-averaged estimated data and monthly-averaged observations, and between daily-averaged estimated data and daily-averaged observations (a) within the ARB for water years 2008-2010, October through June data (to match the WRF period of record), and (b) within the Yosemite area for water years 2003-2005, October through June data.

Smaller interquartile ranges of monthly-averaged dewpoint bias indicate consistent model biases on average, with a range of performance between stations. However, the larger interquartile range in daily-averaged dewpoint bias indicates that there is significant variability in moisture trends both on a daily basis, and between stations in this study location. To highlight this error, we consider that while the *Kunkel* [1989] algorithm only displayed a median bias of 0.1°C in the Yosemite area, the interquartile range of bias values was 4.6°C. Using monthly-averaged data, the PRISM model shows a similarly small range of bias to the WRF model, although it is biased wet in Yosemite. While the assumption that the dewpoint temperature is the minimum air temperature [*Running et al.* 1987] is biased by 1.8°C in the ARB, the interquartile range is 6.3°C. The other empirical algorithms based off temperature showed similar magnitudes of potential error. Radiosonde data is not accurate a large portion of the time, with interquartile bias ranges of 12.3°C in the ARB and 15.2°C in in the Yosemite area. Thus, nearby free air measurements are not an appropriate representation of the basins' moisture the majority of the time. The WRF model is more accurate a greater amount of the time and for a greater number of stations, showing a smaller interquartile range of dewpoint temperature bias, 3.3°C in the ARB and 4.1°C in the Yosemite area.

Furthermore, the performance of the algorithms and models varies seasonally. Figure 7 shows the biases in daily-averaged modelled data for three seasons: the winter (December through February), spring (March through May) and summer (June through August). From this we can observe that biases increase during the summer, dramatically so in the case of radiosonde data. The Yosemite area shows a larger amount of seasonal variation than the more geographically simple ARB.

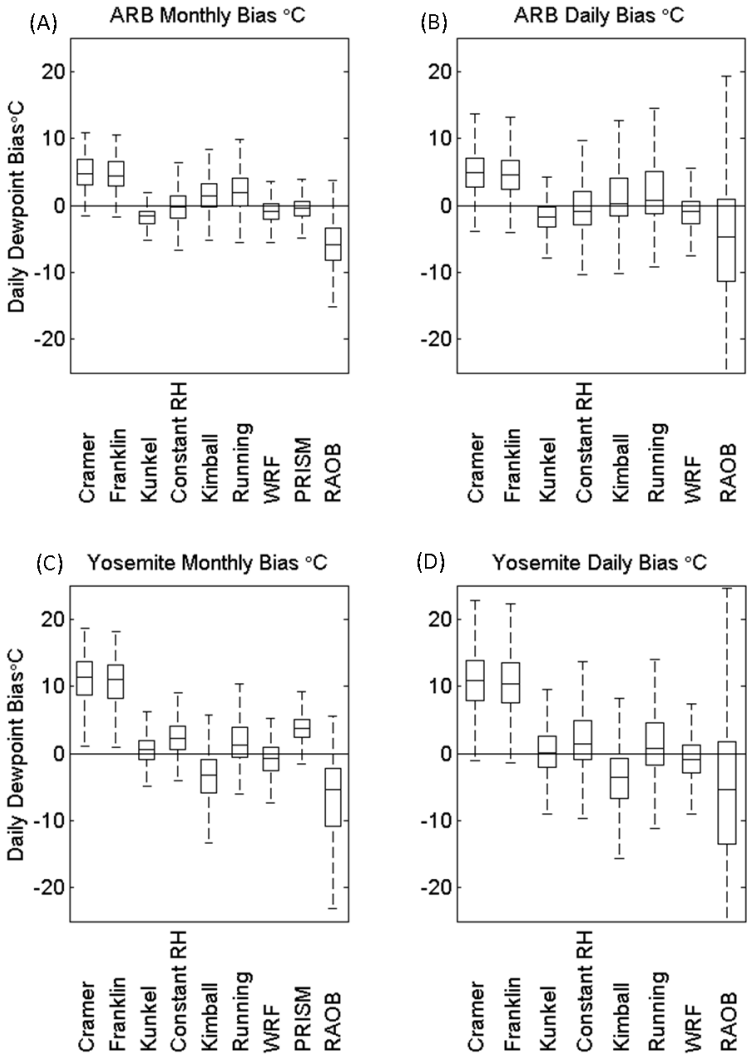

Figure 6. Bias between generated dewpoint temperatures and observations in (A) the American River Basin, monthly-averaged data, (B) the American River Basin, daily-averaged data, (C) Yosemite, monthly-averaged data, (D) Yosemite, daily-averaged data. Methods shown include projections from the Sacramento Airport (constant mixing ratio with elevation [*Cramer*, 1961], -1.25°C/km lapse rate [*Franklin*, 1983], adjustments to vapor pressure [*Kunkel*, 1989], constant RH with elevation [*Wigmosta and Vail*, 1994]), dew point temperatures calculated from air temperature measurements ([*Kimball et al.*, 1997; *Running et al.*, 1987]), the WRF mesoscale model (WRF) [*Skamarock and Klemp*, 2008], PRISM [*Daly et al.*, 2008] and radiosonde data. All data shown is for October through June, for direct comparison with WRF, which was limited to these months.

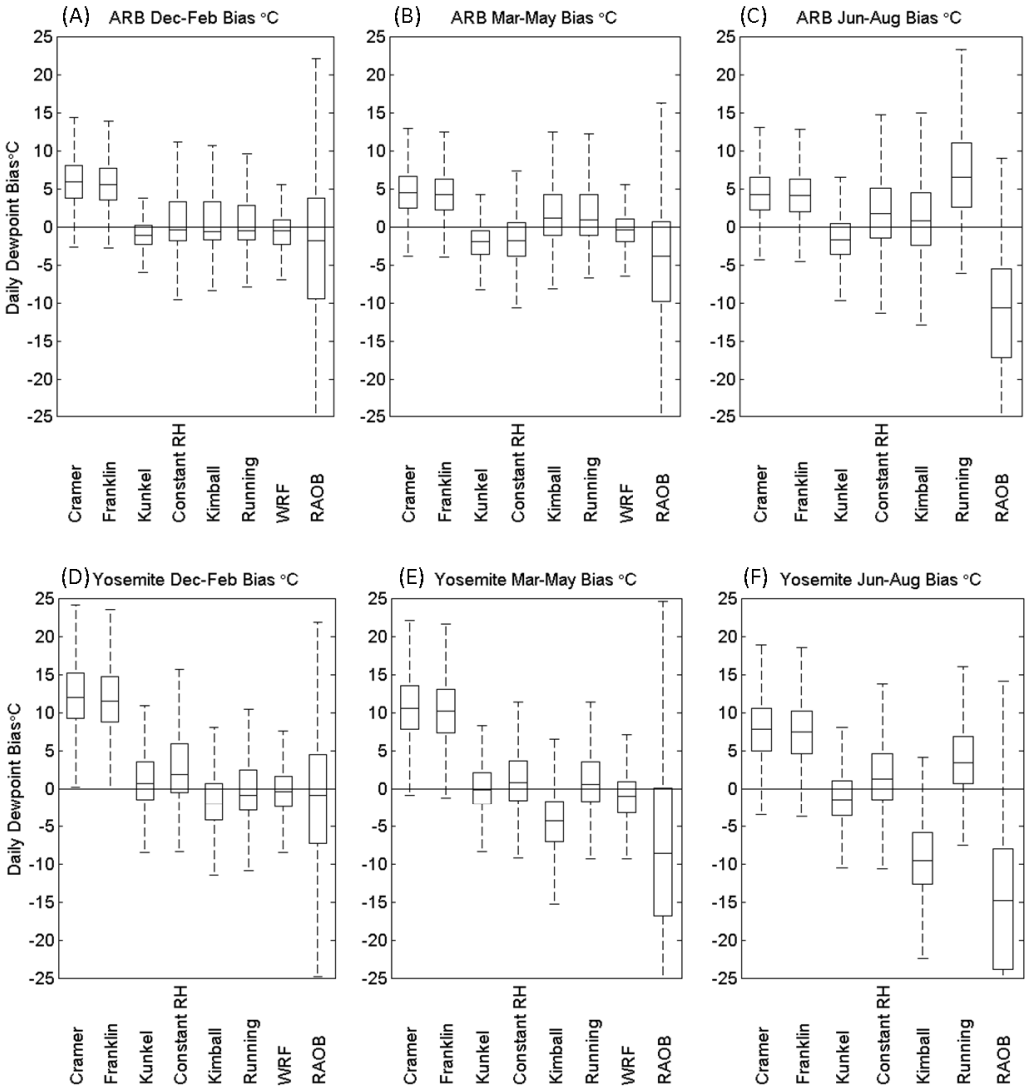

Figure 7. Bias between methods of estimating dewpoint temperature and observations in the American River Basin and Yosemite with daily-averaged data during the winter (Dec-Feb) (A,D), spring (Mar-May) (B,E) and summer (Jun-Aug) (C,F). Methods shown include projections from a low elevation base station (constant mixing ratio with elevation [*Cramer*, 1961], -1.25°C km^{-1} lapse rate [*Franklin*, 1983], adjustments to vapor pressure [*Kunkel*, 1989], constant RH with increases in elevation [*Wigmosta and Vail*, 1994]), dew point temperatures calculated from air temperature measurements ([*Kimball et al.*, 1997; *Running et al.*, 1987]), the WRF mesoscale model (WRF) (unavailable during the summer months) [*Skamarock and Klemp*, 2008], and radiosonde data.

4.3. Factors that Affect Estimation of Dewpoint Temperatures in the Sierra Nevada

As illustrated in Figures 3 and 4, the observed dew point temperature patterns can vary dramatically from one day to the next, so we investigated the mean patterns and which weather patterns lead to deviations from this mean. Averaged annually, moisture declined linearly with elevation in the Sierra Nevada. Median dewpoint temperature changed -5.7°C km^{-1} during days with precipitation and -5.1°C km^{-1} during days without precipitation averaged over water years 2008 through 2010 in the ARB. Median dewpoint temperature changed -7.2°C km^{-1} during days with precipitation and -6.9°C km^{-1} during days without precipitation averaged over water years 2003 through 2005 in the Yosemite area. For reference, the average annual air temperature displayed lapse rates between -6.3 °C km^{-1}in the ARB, and -6.4°C km^{-1} up the west slope of Yosemite. During the summer, moisture changes with elevation were smaller than in the winter. In both regions, dew point temperature lapse rates are on average 2.5°C km^{-1} less during the summer than the winter. This means that there is a smaller moisture decline with increases in elevation in the summer.

While monthly and annually-averaged dew point temperatures varied linearly with changes in elevation, at shorter time periods dew point temperatures often did not show a linear pattern. We determined the fraction of time a lapse rate was a good description of the observed pattern by calculating the RMSE of the observations to the best fit line through those observations, for the ARB, the total Yosemite area, and the Yosemite stations above 1500 meters. In the ARB, dewpoint temperatures generally followed linear trends with elevation, with RMSEs less than 1°C during 35.5% of the study period. In the Yosemite area, RMSEs this small only occurred during 16.5% of the study period. While days with RMSEs>2°C occurred 10.3% of the study period in the ARB, they occurred 25.1% of the study period in the Yosemite area.

Days with RMSEs>3°C occurred during 2% of the study period in the ARB, and 6% of the study period in the Yosemite area. Visual inspections of plots of elevation vs. dewpoint temperature display a breakdown between the dewpoint trends at higher and lower elevation stations in the Yosemite area (Fig. 4). This is illuminated by comparing the RMSEs of the linear fit of all stations in the Yosemite area with that calculated just for stations above 1500 meters. When the analysis was restricted to stations above 1500 m, RMSE values of less than 1°C occurred during 25% of the study period, an improvement over the previous inclusion of low-elevation stations.

We examined how well the data fit a linear approximation as functions of precipitation (Fig. 8A), average relative humidity (Fig. 8B), and dominant wind direction (not shown). Days with rain had smaller RMSE values (Fig. 8A), with median values of 0.7°C in the ARB (253 observations) and 0.9°C in Yosemite (169 observations) as compared to days without rain, median values of 1.3°C in the ARB (820 observations) and 1.6°C in Yosemite (925 observations). Days with a better fit to a linear trend (RMSE<1°C) occurred when RH was closer to saturation (median RH of 85% in the ARB and 80% in Yosemite), while days with a poorer linear trend (RMSE>2°C) were drier (median RH of 45% in the ARB and 44% in Yosemite) (Fig. 8B). In both the ARB and Yosemite, days with a good linear fit between dewpoint temperatures and elevation (RMSE <1°C, 396 days in the ARB, 181 days in Yosemite) occurred in conjunction with strong westerly winds, while days with a weak linear fit between dewpoint temperatures and elevation (RMSE >3°C, 113 days in the ARB, 275 days in Yosemite) occurred during either weak winds or winds off the desert from the east.

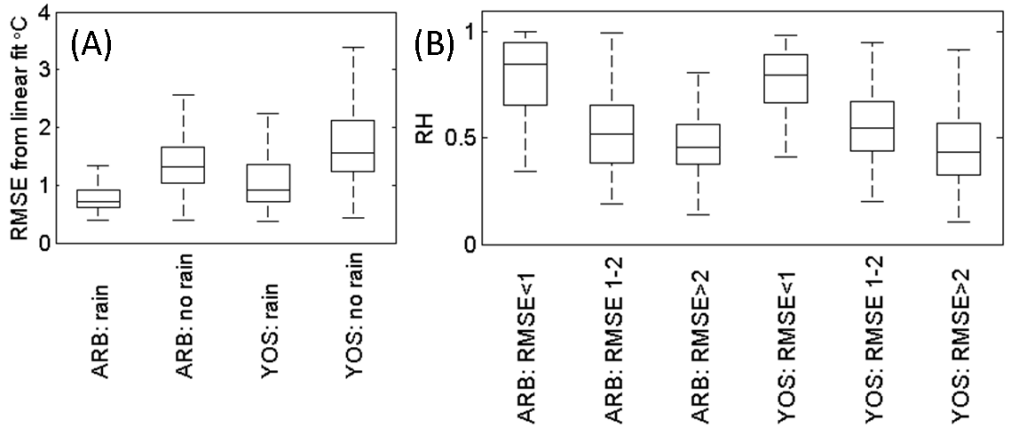

Figure 8. (a) RMSE from a linear dewpoint temperature lapse rate on days with and without rain in the ARB and Yosemite area. (b) RH on days with linear dewpoint lapse rates with gains in elevation (RMSE <1°C), to weak linear trends with elevation (RMSE>2°C) in the ARB and Yosemite.

4.4. Impacts on Hydrology

We demonstrate the impact of dewpoint temperature errors of ±2°C on snow disappearance date and annual streamflow with the DHSVM model calibrated to the Upper Tuolumne River Basin (above Highway 120) during the 7-year period during water years 2003 to 2009. Figure 9A shows the average impacts of a ±2°C dewpoint temperature change to observed dewpoint temperatures over the study period in terms of annual average longwave radiation, annual average latent heat flux, and total annual sublimation. Figure 9B illustrates the impact of a ±2°C dewpoint temperature change for the time period from 1 May to 1 August 2005 on timing of snowmelt and (9C) modeled streamflow. With a 2°C increase in dewpoint temperatures we observed a 2 W m^{-2} increase in estimated longwave radiation, a 0.3 mm day^{-2} decrease in estimated sublimation during the ablation season, snowmelt occurring 3 days earlier, and a 1% increase in modeled cumulative annual streamflow. With a 2°C decrease in dewpoint temperatures, we observed a 2 W m^{-2} decrease in estimated longwave radiation, a 0.2 mm day^{-2} increase in estimated sublimation, snowmelt occurring 3 days later, and a 1% decrease in modeled cumulative annual streamflow.

This is a high-elevation water-limited basin, with a short growing season and little vegetation. Annual evapotranspiration each year is controlled primarily by water availability instead of the energy balance; keeping annual evapotranspiration rates low [*Lundquist and Loheide*, 2011]. In this basin, the primary impacts of dewpoint estimation errors in this basin are on snow, and particularly the sublimation rates. The impact is two-fold in our basin: (a) water is lost due to sublimation, but (b) with the cooling from sublimation latent heat fluxes, the snowpack melts more slowly. In our area, a ±2°C dewpoint temperature shift is on the small side of errors observed. Larger errors in estimation, not shown in this example, further increase the

effects on streamflow and snow disappearance date. Since dewpoint estimation errors increased during the summer, basins with hydrology driven in a larger part by evaporation would see increased model error.

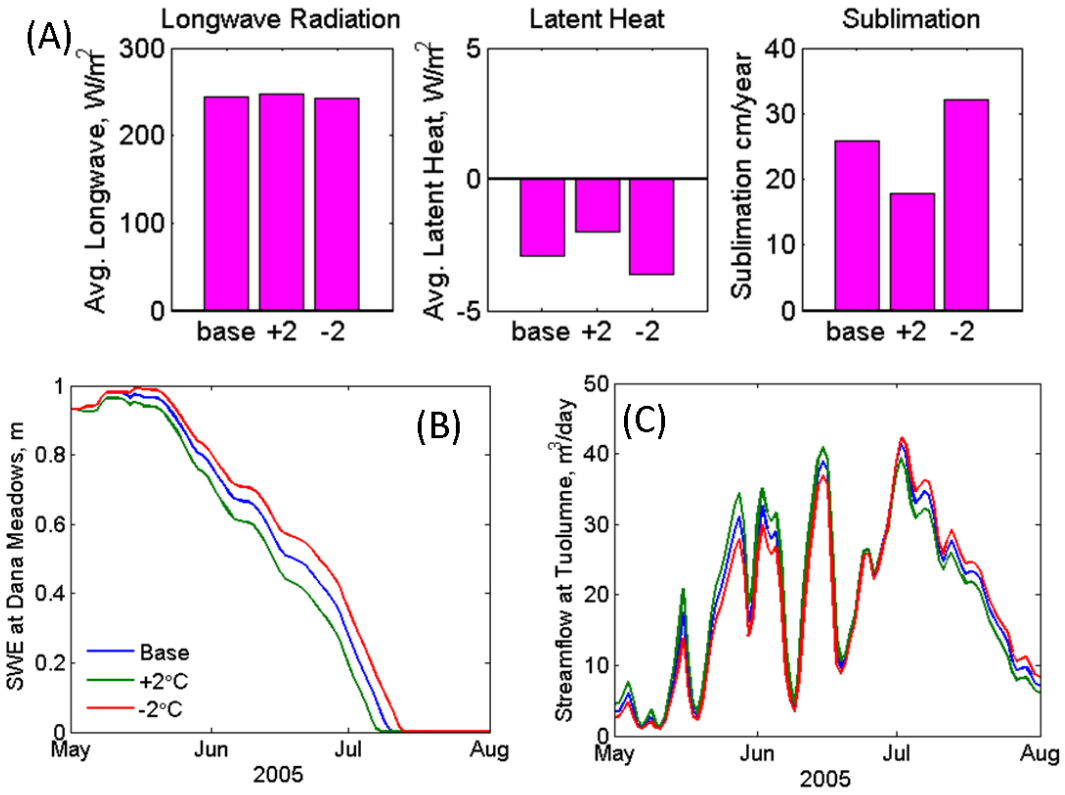

Figure 9. (A) Average annual longwave radiation, latent heat fluxes and calculated sublimation, baseline values and dewpoint changes of ±2°C.(B) Timeseries of SWE at the Dana Meadows snow pillow and (C) annual streamflow in the Tuolumne River above Highway 120 with a ±2°C change in dewpoint temperature.

Table 4. Average annual changes in longwave radiation, latent heat fluxes, daily sublimation rates, streamflow in the TM120 basin and snow disappearance date shift in the upper Tuolumne meadows in Yosemite with a ±2°C change in dewpoint temperature. Sublimation rates are presented for the ablation season.

Dewpoint Change	**+2 °C**	**-2 °C**
Longwave change	2.4 W m^{-2}	-2.3 W m^{-2}
Sublimation change	-8.1 cm $year^{-1}$	6.1 cm $year^{-1}$
Snow disappearance date, Dana Meadows	3 days earlier	3 days later
Net annual Tuolumne River streamflow	1.3%	-1.2%

5. Summary and Discussion

We tested dewpoint estimation methods in the American River Basin and in the Yosemite National Park area in the Sierra Nevada. Empirically-derived lapse rates are typically used to extrapolate one low-elevation dewpoint measurement through the basin. Errors resulted when the lapse rates did not follow the moisture trends within the basin. Both the *Franklin* [1983] assumption of a -1.25°C km^{-1} dewpoint temperature lapse rate and the *Cramer* [1961] assumption of a well-mixed air layer did not result in sufficient moisture declines over the mountain range. Median biases in these methods were up to 10.5°C in the Yosemite area. This indicates that the distribution of moisture with elevation in the Sierra cannot be well-determined by the assumption of an air parcel rising adiabatically along the mountain slope.

Improvements were found with the *Kunkel* [1989] algorithm and the assumption of constant relative humidity, which represent a more rapid rate of moisture decline with elevation. All of the above methods were tested in other regions. PRISM improved upon these methods by using local observations to determine the local lapse rate. However, PRISM was more successful in the ARB (bias = 0.3 °C) than in the Yosemite area (bias = 3.4°C). Dewpoint temperature decreased less rapidly with elevation during the summer, affecting the performance of these empirical methods. The *Franklin* [1983] and *Cramer* [1961] assumptions showed improved performance during the summer, while the assumptions of constant relative humidity and *Kunkel* [1989] performed better during the winter. PRISM performance was consistent across all seasons since it was empirically fit to local data each month.

Empirical algorithms [*Kimball et al.*, 1997; *Running et al.*, 1987] that derived dewpoint from air temperature showed a significant seasonal variation in performance. Both methods were dry-biased on average during the winter in both the ARB and Yosemite. In the more-arid

summer, both methods had wet biases in the ARB (as large as a 8.1°C median bias for the *Running et al.,* [1987] method), but only the Running method was wet biased in Yosemite. The *Kimball et al.,* [1997] aridity correction resulted in a median dry bias of -4.1°C in Yosemite (Fig. 7). These numbers represent a best case scenario for these methods, as we used local temperature at each measurement point to predict the local dewpoint. If the locally-estimated dewpoint must also be projected to another location in the basin (following one of the lapse-based methods described above), the errors are likely to compounded.

Assuming uniform advection of the vertical moisture structure above Oakland (close to the Pacific Ocean) does not well-represent the observed moisture patterns in the Sierra Nevada. Radiosonde readings both showed large biases from observations, and a wide range of day to day error. Dry biases were particularly bad during the summer (median of -11°C in the ARB and -15°C in Yosemite, Fig. 7). During the summer, high pressure and an inversion are common over California, and air is not well-mixed between the Pacific and the Sierra Nevada. Also, transpiration likely increases near-surface moisture relative to the free air at this time of year.

WRF, which used a reanalysis product based on the Oakland sounding data for boundary conditions, greatly improved on the free-air data, performing well in representing both the overall trends in the basin (with median biases of -0.9°C in the ARB and -1.0°C in Yosemite) and displaying the smallest range of error throughout the September through June period. WRF is able to represent cloud dynamics, such as decreases in the dewpoint temperature as precipitation forms and falls out of a saturated air mass (Fig. 3), as well as atmospheric dynamics, such as changing wind speeds and directions (and hence differential moisture advection) with height. For example, different slopes of dewpoint temperature with elevation for groups of stations above and below 1500 m are commonly seen in the Yosemite region (Fig. 4).

This may be due to lower level air being blocked and channeled into a mountain-parallel barrier jet [*Parish*, 1982] while upper level air continues to cross the range from west to east. Or it may be due to mixing of air near the mountain passes with much drier air from the east. While the full dynamics of this pattern are beyond the scope of the present study, WRF is the only methodology examined that consistently represents this change in lapse rate (or curvature) with elevation correctly. One additional advantage of WRF is that it is internally consistent, maintaining physical relations between air temperatures and dewpoint temperatures as water condenses and evaporates. If air temperatures and dew point temperatures are independently calculated from empirical lapse rates, the possibility exists for extrapolated dew point temperatures to exceed air temperatures, which would be an implausible representation of supersaturated air due to the neglect of calculating moisture condensation.

Empirical models that use projections from a point measurement assume that dewpoint temperatures follow a linear trend with elevation. This assumption was valid only part of the time at our study sites. Days with a RMSE of <1°C to a linear fit occurred 35.5% of the time in the ARB, but only 16.5% of the study period in the Yosemite area. Linear dewpoint temperature trends were more likely during predominant westerly winds and/or on days with precipitation or high humidity. Due to the separation in slope in the Yosemite dataset (described above and illustrated in Fig. 4), the frequency of a RMSE of <1°C to the linear fit increased from 16.5% to 25% when we restricted analysis to stations above 1500 meters elevation. The southern Sierra Nevada extends to higher elevations than the northern Sierra Nevada, resulting in more frequent blocking of wind, which is channeled into barrier jets along the mountain range [*Lundquist et al.*, 2010]. Thus, low elevation sites are exposed to air advected from low elevations to the south, whereas higher elevation sites are more likely exposed to air advected from the west. This flow

separation sets up moisture influences at higher elevations that differ from lower elevations, resulting in a break in the linear lapse rate. Thus in complex terrain, significant improvements in these modeling representations can be made by running WRF, which captures these dynamics, or by including enough higher-elevation base stations to resolve the observed changes in the dew point lapse rate.

We tested the effects of dewpoint estimation errors of ±2°C on streamflow simulations in a high elevation basin (>2600 m) within our Yosemite study area. Because this area is snowmelt driven, the primary impacts of dewpoint errors were on the snowpack simulation. Higher dewpoints increased estimates of downwelling longwave radiation (from the higher moisture content and hence, emissivity, of the atmosphere) and decreased modeled sublimation (by decreasing the vapor pressure deficit), which in turn, resulted in less cooling from the accompanying latent heat flux. The net effect was an increase in melt rates and a shift in streamflow timing towards earlier in the year (Fig. 9). Lower dewpoints had the opposite effect on each process, resulting in slower melt and later streamflow timing (Fig. 9). While the overall effects of ±2°C biases were not large (± 3 days shift in snow disappearance), many of the methods tested resulted in much larger dewpoint biases for this basin (+10°C for the Cramer and Franklin methods and -4°C for the Kimball method), which would have larger impacts on snow and melt timing.

Most of the Sierra Nevada is moisture-limited, and so, while streamflow and net annual evapotranspiration are likely not sensitive to dewpoint temperature errors, many ecological processes likely will be. For example, the vapor pressure deficit is a critical parameter in determining fire danger, and many ecological communities are sensitive to desiccation when the vapor pressure drops below a critical value [*Rorig and Ferguson,* 1999; *Grantz*, 1990]. Errors in

estimating dewpoint temperatures increased in the summer for most methods (Fig. 7), and these errors are likely to have broader reaching impacts than those we illustrated here for snow.

6. Conclusions

In sum, our results indicate that (1) empirical assumptions calibrated for other study sites may not be appropriate in the Sierra Nevada, (2) the assumption of a linear trend of dewpoint temperatures with gains in elevation is not always appropriate in the Sierra Nevada, and (3) the WRF model significantly improves on both free-air readings and empirical techniques in representing dewpoint temperatures within the basin. The geographic differences between the two study sites were illuminated by the poorer performance of algorithms in the Yosemite area.

Our study highlights the importance of both observations within a basin, and recognizing topographic limits on the use of simple models. If you are modeling a geographically simple basin such as the ARB, one base station within the basin paired with PRISM lapse rates will be representative of overall moisture trends most of the time. However, if the basin is more geographically complex, with air masses not only due to predominant weather patterns, but micro-topography effects and transport along the mountain range, a physically-resolved model such as WRF is necessary to represent dewpoint variations. If one is just concerned with reducing the average modeled bias in a basin, the simplest method is to add a high-elevation station that records dewpoint temperatures and use a model that represents dew point temperature declining with elevation.

7. Appendix A: Atmospheric Moisture Metrics and Calculations

We outline metrics used to determine atmospheric moisture content and how we calculated dewpoint temperature. The actual amount of water in the air can be viewed as the mixing ratio (*r, g/kg or kg/kg*), which is the ratio of the mass of water to the mass of dry air. The amount of water in the air can also be given as the actual vapor pressure (*e, Pa*) of water in the air. This relates to the mixing ratio and local air pressure (*p, Pa*) through the equation [*Glickman and American Meteorological Society*, 2000]:

$$r = \frac{0.622e}{p - e} \tag{1}$$

At a given temperature, there is potential for the atmosphere to hold a given amount of water. This maximum water vapor that the air can hold, called the saturation vapor pressure (e_s, *Pa)*, is defined by the pressure and temperature dependence of the relation between the liquid and gas phases of water. A large number of methods have been proposed to determine the saturation vapor pressure from air temperature (*T, °C*) based on empirical or theoretical derivations [*Lawrence*, 2005]. We employ the Magnus-Tetens formula [*Murray et al.*, 1967] with empirically updated coefficients [*Alduchov and Eskridge*, 1996]. The formula, shown here, was found to err less than 0.4% for the temperature range of -40°C to 50°C [*Lawrence*, 2005].

$$e_s = 610.94(Pa)\exp\left(\frac{17.625T}{243.04°C + T}\right) \tag{2}$$

In hydrological applications, we are often concerned with the ratio of the amount of water in the atmosphere over the amount of water that the atmosphere can hold. This ratio is called the relative humidity (*RH, %*), and can be defined as:

$$RH = 100\frac{e}{e_s} \tag{3}$$

The dew point temperature (T_d, $°C$) is the temperature at which the air will be saturated for a given amount of water vapor. This can be calculated from the actual amount of water vapor in the air (e) as determined from relative humidity and the Magnus formulation for vapor pressure at the dewpoint temperature:

$$T_d = \frac{243.04°C \ln\left(\frac{e}{610.94}\right)}{17.625 - \ln\left(\frac{e}{610.94}\right)} \tag{4}$$

This can be solved to a formulation the takes inputs of commonly measured variables, relative humidity and air temperature:

$$T_d = \frac{243.04°C\left[\ln\left(\frac{RH}{100}\right) + \frac{17.625T}{243.04°C + T}\right]}{17.625 - \ln\left(\frac{RH}{100}\right) - \frac{17.625T}{243.04°C + T}} \tag{5}$$

The dewpoint depression can be used to view the measure of the difference between actual and potential water vapor content in terms of temperatures. This is calculated as the dewpoint temperature subtracted from the air temperature.

8. Appendix B: Reference for Processing Hygrochron Data

In the hygrochron, temperature is measured with a digital thermometer. For RH readings, a small hole covered with a filter permits only water vapor to enter, which is then measured with a capacitance sensor. The instrument can be programmed to take readings at specified intervals ranging from one second to 273 hours, with an optional recording start delay. The device has a storage capacity of 8192 8-bit readings or 4096 16-bit readings; this corresponds to roughly 11 months of 8-bit temperature and RH readings taken at 2 hour intervals. The operating range of the instrument is between -20 and 85°C with an accuracy of 0.5°C, and 0 and 100% humidity with an accuracy of 5%. The minimum listed lifetime when logging both temperature and RH every hour in temperatures of -10°C to 40°C is between 6 and 7.5 years [Maxim datasheet, Report 19-4991, Rev 3, October 2009]. The HMP45s used for comparison have a stated accuracy of 2% RH when the humidity is less than 90%, and 3% otherwise [Campbell datasheet, Model HMP45C Temperature and Relative Humidity Probe, Rev March 2009]. The hygrochron data can be read with a USB computer attachment and software downloaded from the manufacturer's website.

The currently available software for processing hygrochrons is the OneWireViewer program. When using the OneWireViewer software, the capacitance measurement of RH assumes a temperature of 25°C. This must be converted to the correct relative humidity using the temperature data and the following conversion:

$$HT_{corr} = \frac{H_{corr}K + \alpha(T - 25°C) - \beta(T - 25°C)^2}{K + \gamma(T - 25°C) - \delta(T - 25°C)^2} \quad (6)$$

Where H_{corr} is the humidity reading with an applied software correction algorithm that is included in the OneWireViewer data processing, T is the temperature in °C, K is 0.0307, α is $0.0035°C^{-1}$, β is $0.000043°C^{-2}$, γ is $0.00001°C^{-1}$ at temperatures greater than 15°C and -0.00005°C at temperatures less than 15°C, and δ is $0.000002°C^{-2}$ as can be found in the manufacturer's datasheet (Maxim datasheet, Report 19-4991).

When hygrochrons are exposed to humidity above 70% for prolonged periods of time, the sensors tend to record higher than actual values. This is called saturation drift, and can be corrected for all cases when the readings exceed 70% RH using the following compensation:

$$HS_{corr} = HTN_{corr} - \sum_{k=1}^{N} \frac{0.0156 HT_{corr} * 2.54^{-0.3502k}}{1 + (T_k - 25)/100} \quad (7)$$

where HS_{corr} is the humidity reading after the drift compensation, N is the number of hours that the hygrochron records values greater than 70% humidity, HTN_{corr} is the temperature compensated humidity reading at the end of the N^{th} hour, HT_{corr} is the temperature compensated humidity reading at the k^{th} hour, and T_k is the temperature reading at the k^{th} hour.

The user is encouraged to check with the manufacturer for updates to the software or data correction procedures.

9. References

Alduchov, O.A., and R.E. Eskridge (1996), Improved Magnus Form Approximation of Saturation Vapor Pressure, *Journal of Applied Meteorology*, *35*, 601–609.

Barnett, T.P., Pierce, D.W., Hidalgo, H.G., Bonfils, C., Santer, B.D., Das, T., Govindasamy, B., Wood, A.W., Nozawa, T., Mirin, A.A., Cayan, D.R., Dettinger, M. D. (2008), Human-Induced Changes in the Hydrology of the Western United States, *Science*, *319*(5866), 1080–1083.

Cramer, O. (1961), Adjustment of Relative Humidity and Temperature for Differences in Elevation, *USDA For. Serv., Pac. Northwest For. Range Exp. Stn., Portland, OR*, *Res. Pap. 43*.

Cristea, N., and J. D. Lundquist (submitted), Evaluating streamflow timing and magnitude in the upper Tuolumne basin, Sierra Nevada, as a response to climate changes and forest cover.

Dai, A., G.A Meehl, W.W. Washington, T. M. L. Wigley, and J.M. Arblaster (2001), Ensemble Simulation of Twenty-First Century Climate Changes : Business- as-Usual versus CO 2 Stabilization, *Bulletin of the American*, *82*(11), 2377–2388.

Daly, C., M. Halbleib, J.I. Smith, W.P. Gibson, M.K. Doggett, G.H. Taylor, J. Curtis, and P. Pasteris (2008), Physiographically sensitive mapping of climatological temperature and precipitation across the conterminous United States, *International Journal of Climatology*, *28*, 2031–2064, doi:10.1002/joc.

Daly, C., R.P. Neilson, and D.L. Phillips (1994), A statistical-topographic model for mapping climatological precipitation over mountainous terrain, *Journal of Applied Meteorology*, *33*(2), 140–158.

Dodd, A. V. (1965), Dew Point Distribution in the Continguous United States, *Monthly Weather Review*, *93*(2), 113–122.

Eccel, E. (2012), Estimating air humidity from temperature and precipitation measures for modelling applications, *Meteorological Applications*, *19*(1), 118–128, doi:10.1002/met.258.

Flerchinger, G. N., W. Xaio, D. Marks, T. J. Sauer, and Q. Yu (2009), Comparison of algorithms for incoming atmospheric long-wave radiation, *Water Resources Research*, *45*(3), 1–13, doi:10.1029/2008WR007394.

Finklin, A.I. 1983. Climate of the Priest River experimental forest, northern Idaho. *USDA, Forest Service,* Gen. Tech. Rep. INT-159.

Gaffen, D. J., and R. J. Ross (1999), Climatology and Trends of U . S . Surface Humidity and Temperature, *Journal of Climate*, *12*, 811–828.

Glassy, J. M., and S. W. Running (1994), Validating diurnal climatology logic of the MT-CLIM model across a climatic gradient in Oregon, *Ecological Applications*, *4*(2), 248–257.

Glickman, T. S., and American Meteorological Society (2000), *Glossary of meteorology*, 2nd ed., American Meteorological Society.

Grantz, D.A. (1990), *Plant response to atmospheric humidity*, Plant, Cell & Environment, 13,667-679. doi: 10.1111/j.1365-3040. 1990.tb01982.x

Gong, L., C. Xu, D. Chen, S. Halldin, and Y. D. Chen (2006), Sensitivity of the Penman–Monteith reference evapotranspiration to key climatic variables in the Changjiang (Yangtze River) basin, *Journal of Hydrology*, *329*(3-4), 620–629, doi:10.1016/j.jhydrol.2006.03.027.

Hamlet, A.F., Lettenmaier, D. P. (2005), Production of Temporally Consistent Gridded Precipitation and Temperature Fields for the Continental United States, *Journal of Hydrometeorology*, *6*, 330–336.

Hughes, M., P.J. Neiman, E. Sukovich, and F.M. Ralph (2012), Representation of the Sierra Barrier Jet in 11 years of a high-resolution dynamical reanalysis downscaling compared with long-term wind profiler observations, conditionally accepted to *JGR-Atmospheres.*

Idso, S. (1981), A set of equations for full spectrum and 8-to 14-Î¼m and 10.5-to 12.5-Î¼m thermal radiation from cloudless skies, *Water resources research*, *17*(2), 295, doi:10.1029/WR017i002p00295.

Ivanov, V. Y., E.R. Vivoni, R.L. Bras, D. Entekhabi (2004), Catchment hydrologic response with a fully distributed triangulated irregular network model, *Water Resources Research*, *40*(11), 11102, doi:10.1029/2004WR003218.

Ivanov, V. Y., R. L. Bras, and D. C. Curtis (2007), A weather generator for hydrological, ecological, and agricultural applications, *Water Resources Research*, *43*(10), doi:10.1029/2006WR005364.

Kimball, J. S., S. W. Running, and R. Nemani (1997), An improved method for estimating surface humidity from daily minimum temperature, *Agricultural and Forest Meteorology*, *85*, 87–98.

Kunkel, K. (1989), Simple procedures for the extrapolation of humidity variables in the mountainous Western United States, *Journal of climate*, *2*, 656–669.

Lawrence, M. G. (2005), The Relationship between Relative Humidity and the Dewpoint Temperature in Moist Air: A Simple Conversion and Applications, *Bulletin of the American Meteorological Society*, *86*(2), 225–233, doi:10.1175/BAMS-86-2-225.

Liang, X., D. P. Lettenmaier, E.F. Wood, and S.J. Burgess (1994), A simple hydrologically based model of land surface water and energy fluxes for general circulation models, *Joumal of Geophysical Research 99D7*, *99*(D7), 14,415–14,428.

Liston, G.E., and K. Elder (2006), A meteorological distribution system for high-resolution terrestrial modeling (MicroMet), *Journal of Hydrometeorology*, *7*, 217–234.

Lowry, C. S., S. P. Loheide, C. M. Moore, and J. D. Lundquist (2011), Groundwater controls on vegetation composition and patterning in mountain meadows, *Water Resources Research*, *47*(W00J11), doi:10.1029/2010WR010086.

Lundquist, J.D., D.R. Cayan, and M.D. Dettinger (2003), Meteorology and hydrology in yosemite national park: A sensor network application, in *Proceedings of the 2nd International Symposium on Information Processing in Sensor Networks*, pp. 518–528.

Lundquist, J. D., and D. R. Cayan (2007), Surface temperature patterns in complex terrain: Daily variations and long-term change in the central Sierra Nevada, California, *Journal of Geophysical Research*, *112*(D11), 1–15, doi:10.1029/2006JD007561.

Lundquist, J. D., and B. Huggett (2008), Evergreen trees as inexpensive radiation shields for temperature sensors, *Water Resources Research*, *44*, 1–5, doi:10.1029/2008WR006979.

Lundquist, J. D., and S. P. Loheide (2011), How evaporative water losses vary between wet and dry water years as a function of elevation in the Sierra Nevada, California, and critical factors for modeling, *Water Resources Research*, *47*, W00H09, doi:10.1029/2010WR010050.

Lundquist, J. D., J. R. Minder, P.J. Neiman, and E. Sukovich (2010), Relationships between Barrier Jet Heights, Orographic Precipitation Gradients, and Streamflow in the Northern Sierra Nevada, *Journal of Hydrometeorology*, *11*(5), 1141–1156, doi:10.1175/2010JHM1264.1.

Lundquist, J. D., P. J. Neiman, B. Martner, A. B. White, D. J. Gottas, and F. M. Ralph (2008), Rain versus Snow in the Sierra Nevada, California: Comparing Doppler Profiling Radar and Surface Observations of Melting Level, *Journal of Hydrometeorology*, *9*(2), 194–211, doi:10.1175/2007JHM853.1.

Maurer, E.P., Wood, A.W., Adam, J.C., Lettenmaier, D. P. (2002), A Long-Term Hydrologically Based Dataset of Land Surface Fluxes and States for the Conterminous United States, *American Meteorological Society*, *15*, 3237–3251.

Meek, DW, J.L. Hatfield (1994), Data quality checking for single station meteorological databases, *Agricultural and forest meteorology*, *69*(1-2), 85–109.

Mesinger, F., G. DiMego, E. Kalnay, K. Mitchell, P.C. Shafran, W. Ebisuzaki, D. Jovic, J. Woollen, E. Rogers, E.H. Berbery, M.B. Ek, Y. Fan, R.Grumbine, W. Higgins, H. Li, Y. Lin, G. Manikin, D. Parrish, W. Shi (2006), North American Regional Reanalysis, *Bulletin of the American Meteorological Society*, *87*(3), 343–360, doi:10.1175/BAMS-87-3-343.

Morrison, H., G. Thompson, V. Tatarskii (2009), Impact of Cloud Microphysics on the Development of Trailing Stratiform Precipitation in a Simulated Squall Line: Comparison of One- and Two-Moment Schemes, *Monthly Weather Review*, *137*(3), 991–1007, doi:10.1175/2008MWR2556.1.

Murray, F. W. (1967), On The Computation of Saturation Vapor Pressure, *Journal of Applied Meteorology*, *6*, 203–204.

NOAA (1968), *Climatic Atlas of the United States*.

Peel, M.C., B.L. Finlayson, and T.A. McMahon (2007), Updated world map of the Koppen-Geiger climate classification, *Hydrology and Earth System Science*, *11*, 1633–1644.

Rangwala, I., J.R. Miller, G. L. Russell, and M. Xu (2009), Using a global climate model to evaluate the influences of water vapor, snow cover and atmospheric aerosol on warming in the Tibetan Plateau during the twenty-first century, *Climate Dynamics*, *34*(6), 859–872, doi:10.1007/s00382-009-0564-1.

Robinson, P. J. (1998), Monthly variations of dew point temperature in the coterminous United States, *International Journal of Climatology*, *18*(14), 1539–1556, doi:10.1002/(SICI)1097-0088(19981130) 18:14<1539::AID-JOC326>3.0.CO;2-L.

Robinson, P. J. (2000), Temporal trends in United States dew point temperatures, *International Journal of Climatology*, *20*(9), 985–1002, doi:10.1002/1097-0088(200007)20:9<985::AID-JOC513>3.0.CO;2-W.

Rorig, M.L., S.A. Ferguson (1999), Characteristics of lightning and wildland fire ignition in the Pacific Northwest, *J. Appl. Meteorology,* 38, 1565-1575.

Ruckstuhl, C., R. Philipona, J. Morland, and A. Ohmura (2007), Observed relationship between surface specific humidity, integrated water vapor, and longwave downward radiation at different altitudes, *Journal of Geophysical Research*, *112*(D3), 1–7, doi:10.1029/2006JD007850.

Running, S. W., R. Nemani, and R. Hungerford (1987), Extrapolation of synoptic meteorological data in mountainous terrain, and its use for simulating forest evapotranspiration and photosynthesis, *Canadian Journal Of Forest Research*, *17*, 472–483.

Sicart, J. E., J. W. Pomeroy, R. L. H. Essery, and D. Bewley (2006), Incoming longwave radiation to melting snow : observations , sensitivity and estimation in northern environments, *Hydrological Processes*, *20*, 3697–3708, doi:10.1002/hyp.

Skamarock, W. C., and J. B. Klemp (2008), A time-split nonhydrostatic atmospheric model for weather research and forecasting applications, *Journal of Computational Physics*, *227*, 3465–3485, doi:10.1016/j.jcp.2007.01.037.

Tague, C., and L. Band (2004), RHESSys : Regional Hydro-Ecologic Simulation System — An Object- Oriented Approach to Spatially Distributed Modeling of Carbon , Water , and Nutrient Cycling, *Earth Interactions*, *8*(19), 1–42.

Trenberth, K. E., and C. (2007), Observations: Surface and atmospheric climate change, in *Climate Change 2007: The Physical Science Basis*, edited by H. L. Solomon, S., Qin, D., Manning, M., Chen, Z., Marquis, M., Averyt, K.B., Tignor, M., Miller, pp. 235–336, Cambridge University Press.

Waichler, S. R., and M. S. Wigmosta (2003), Development of Hourly Meteorological Values From Daily Data and Significance to Hydrological Modeling at H. J. Andrews Experimental Forest, *Journal of Hydrometeorology*, *4*(2), 251–263, doi:10.1175/1525-7541(2003)4<251:DOHMVF>2.0.CO;2.

Wallace, J. M., and P. V. Hobbs (2006), *Atmospheric Science, Second Edition: An Introductory Survey (International Geophysics)*, 2nd ed.

Wayand, N. E., A. F. Hamlet, M. Hughes, S. I. Feld, and J. D. Lundquist (submitted), Intercomparison of Meteorological Forcing Data from Empirical and Mesoscale Model Sources in the N.F. American River Basin in northern California, *submitted to Journal of Hydrometeorology*.

Wigmosta, M.S., L.W Vail, D.P. Lettenmaier (1994), A distributed hydrology-vegetation model for complex terrain, *Water Resources Research*, *30*(6), 1665–1679.